phys. stat. sol. (b) **224**, No. 1, 147–151 (2001)

Cd Distribution and Defects in Single and Multilayer CdSe/ZnSe Quantum Dot Structures

D. Litvinov[1]) (a), D. Gerthsen (a), A. Rosenauer (a), H. Preis (b), E. Kurtz (c), and C. Klingshirn (c)

(a) Labor für Elektronenmikroskopie, Universität Karlsruhe, D-76128 Karlsruhe, Germany

(b) Institut für Experimentelle und Angewandte Physik, Universität Regensburg, D-93040 Regensburg, Germany

(c) Institut für Angewandte Physik, Universität Karlsruhe, D-76128 Karlsruhe, Germany

(Received July 31, 2000; accepted October 2, 2000)

Subject classification: 61.72. Ff; 68.35. Dv; 68.65.Hb; S8.12

Conventional and high-resolution transmission electron microscopy (TEM) was applied to a study of the Cd distribution and structure of defects in single and multiple CdSe layers in a ZnSe matrix. The samples containing nominal CdSe layer thicknesses t_n between 1.7 and 3.5 monolayers (ML) were grown by molecular beam and atomic layer epitaxy under different conditions. In all samples ternary CdZnSe wetting layers with Cd-rich regions with sizes of less than 10 nm (small islands: SIs) and a density of $\sim 10^{11}$ cm^{-2} are observed. The Cd concentration in the wetting layer and the SIs increase with t_n. In addition, regions with sizes of 20–30 nm (large islands: LIs) and Cd concentrations >40% occur in specimens with $t_n > 2.5$ ML. In the vicinity of the LIs stacking faults are preferably generated leading to a "coffee-bean" contrast in plan-view TEM images. The multilayer structures with $t_n \approx 2.5$ ML display a predominant vertical correlation of the SIs at a ZnSe spacer thickness of 12 ML.

1. Introduction A considerable number of studies about CdSe/ZnSe quantum dot (QD) structures were recently carried out which are motivated by the perspective of incorporating QD structures in laser diodes for the blue-green spectral range. The co-existence of two size classes of self-organized islands was previously observed [1–3]. Cd-rich regions with a size of less than 10 nm (small islands: SIs) appear even at nominal thicknesses $t_n < 1$ monolayer (ML) which are embedded in a broadened wetting layer (WL) [2–5]. Large three-dimensional islands (LIs) with sizes of significantly above 10 nm occur at larger t_n in the range of 2.1–3 ML [1–3] whose origin can be associated with a transition from the two-(2D) to the three-dimensional (3D) growth mode. Krestnikov et al. [5] investigated CdSe/ZnSe superlattices with $t_n < 1$ ML and varying thicknesses of the ZnSe spacer and found a vertical correlation of the Cd-rich inclusions for thin (1.5 nm) ZnSe spacers. In the present paper we present a transmission electron microscopy (TEM) study of the structural and chemical properties of single CdSe/ZnSe structures with different t_n and multiple CdSe/ZnSe structures with $t_n \approx 2.5$ ML and various ZnSe spacers.

2. Experimental Setup Three types of samples were investigated. The first type (samples 1) was grown by standard molecular beam epitaxy at a temperature $T_s = 400$ °C.

[1]) Corresponding author; Tel.: (+49) (721) 6084889; Fax: (+49) (721) 6083721; e-mail: litvinov@lem.uni-karlsruhe.de

The samples 1 consist of a strained ZnSe buffer layer of 20 nm thickness grown on a (001)-oriented GaAs substrate, a single CdSe layer with $1.7\ \mathrm{ML} \le t_n \le 3.0\ \mathrm{ML}$ and a 20 nm thick ZnSe cap layer. The three-stack CdSe/ZnSe structures (samples 2) were grown as the samples 1 with a 5 s growth interruption after the CdSe deposition. They contain CdSe with $t_n = 2.5$ ML and ZnSe spacers with thicknesses t_{ZnSe} of 10, 12, 15 or 20 ML. The third type of samples (samples 3) was grown at $T_s = 230\ ^\circ\mathrm{C}$ by atomic layer epitaxy with subsequent annealing at 340 °C after the deposition of 3.5 ML CdSe. In this case the ZnSe buffer and cap layer thicknesses were 120 and 20 nm, respectively. The growth was controlled by in-situ monitored reflection high energy electron diffraction (RHEED) patterns. The structural properties were studied by TEM performed on plan-view (PV) and cross-section samples along the [010]-, [110]- and $[1\bar{1}0]$-zone axes. The Cd contribution in the cross-section samples was quantitatively measured by the CELFA (composition evaluation by lattice fringe analysis) procedure [6] and by the evaluation of (002) two-beam dark-field images [3]. Both techniques are based on the chemical sensitivity of the (002) reflection in the zincblende structure.

3. Experimental Results The investigation of the Cd distribution by CELFA shows that (instead of binary CdSe layers) ternary CdZnSe WLs with a thickness of $\approx$3 nm are observed in all samples independent of t_n which contain Cd-rich regions (SIs) with sizes of less than 10 nm and a density of $\sim 10^{11}\ \mathrm{cm}^{-2}$. Table 1 summarizes the measured average integrated CdSe content, Cd concentration x_{Cd} and integrated CdSe content in the WL and the SI for the samples 1 with different t_n. The ratios of CdSe content and x_{Cd} in the SI and WL are $\sim$1.5 for the specimens with $t_n = 1.7$ and 3.0 ML and $\sim$1.8 for $t_n = 2.5$ ML. The errors are statistical errors representing the variation of the data in different sample regions.

RHEED observations during the CdSe growth reveal the change from a streaky to a spot-like pattern in the samples 1 with $t_n > 2.5$ ML which is associated with a 2D/3D growth-mode transition. The same transition occurs for the samples 3 during the annealing step. Cross-section images of these samples (not shown here) reveal LIs with sizes between 20 and 30 nm containing $x_{Cd} > 40\%$ and integrated CdSe contents >5 ML. In the PV strong-beam TEM images of samples containing LIs, regions with a "coffee-bean" contrast appear. Figures 1a–c show typical PV TEM images of the sample 3 taken under various imaging conditions. The [001]-zone axis bright-field image Fig. 1a depicts "coffee-bean" regions with a density $5 \times 10^{10}\ \mathrm{cm}^{-2}$. The (220) weak-beam (WB) image Fig. 1b reveals the stripe contrast of stacking faults (SFs). Two pairs of partial dislocations (PDs) with a V-shaped dislocation line arrangement are observed in the

Table 1
Nominal and measured average CdSe content, integrated CdSe content and Cd concentration in the SIs and WL obtained by CELFA for the samples 1 with different t_n

average CdSe content (ML)		CdSe content (ML)		Cd concentration (%)	
nominal	measured	WL	SI	WL	SI
1.7	1.3 ± 0.1	1.1 ± 0.1	1.6 ± 0.1	17 ± 1	23 ± 3
2.5	2.2 ± 0.2	1.5 ± 0.1	2.8 ± 0.2	20.5 ± 2.5	37 ± 1
3.0	2.8 ± 0.2	2.3 ± 0.1	3.6 ± 0.4	23.5 ± 1.5	32 ± 3

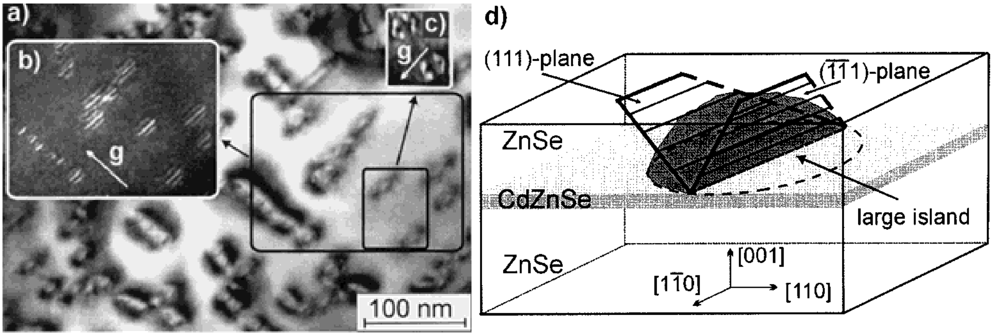

Fig. 1. a)–c) Plan-view TEM images of the sample 3 taken under different imaging conditions and d) schematic drawing of the defect configuration

(2$\bar{2}$0) WB image (Fig. 1c). Using different imaging vectors **g** and taking into account the results of cross-section investigations in the [110], [1$\bar{1}$0] and [010] projections the defect configuration is obtained which is shown in Fig. 1d. Two SFs on inclined {111} planes occur which are bounded by Shockley PDs with Burgers vectors **b** of the type 1/6 ⟨112⟩. A stair-rod PD with **b** = 1/6 ⟨110⟩ perpendicular to the dislocation line is generated at the intersection of the two SFs. The SF width decreases close to the ZnSe cap-layer surface. The cross-section images (not shown here) indicate that the SFs are preferably generated close to LIs where high $x_{Cd} > 40\%$ and CdSe contents >5 ML are measured.

In Fig. 2 (200) cross-section dark-field images of the three-stack structures (samples 2) with different t_{ZnSe} are presented. The CdSe layers can be identified by their lower brightness which is induced by the chemical sensitivity of the (200) reflection.

For $t_{ZnSe} = 10$ ML we receive one broad intermixed CdZnSe layer. Regions with vertically correlated SIs in the sample with $t_{ZnSe} = 12$ ML are marked by arrows. The correlation of the SIs disappears for $t_{ZnSe} \geq 15$ ML.

4. Discussion Two types of islands and a strongly broadened ternary CdZnSe WL are observed in the CdSe/ZnSe structures depending on t_n. SIs with sizes ≤10 nm are obtained in all samples. The integrated CdSe content and x_{Cd} in the WL and the SIs

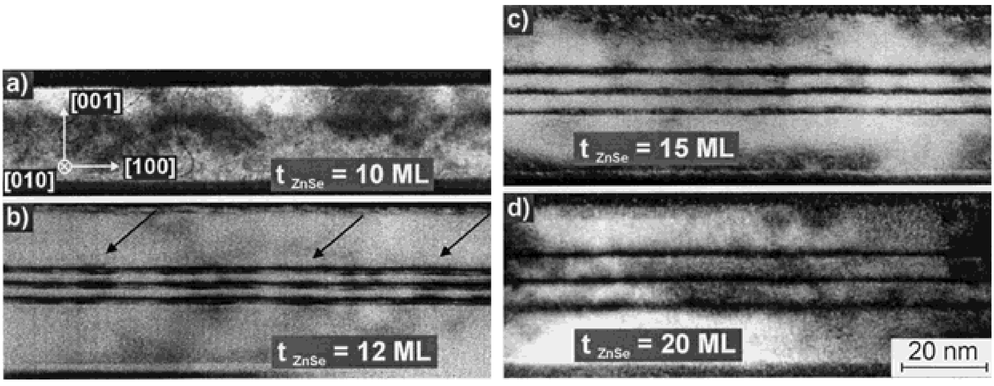

Fig. 2. (200) TEM dark-field cross-section images of the three stack samples 2 with different thicknesses of ZnSe spacer

increase with t_n (Table 1) without a significant change of the actual WL thickness. It is quite remarkable that the same type of Cd distribution (SIs in a strongly broadened WL with a thickness of about 3 nm) occurs in structures which are grown in different MBE systems by applying completely different growth modes and conditions (see also [2–5]).

The second island type is associated with a 2D/3D growth-mode transition which occurs at $t_n \approx 2.5$ ML depending on the actual growth conditions. The LIs contain high x_{Cd} and integrated CdSe contents. SFs with a configuration shown in Fig. 1d are frequently observed in the vicinity of the LIs where the stair-rod dislocation could act as a misfit-relieving dislocation. A detailed mechanism for the defect generation cannot yet be proposed. However, it is plausible that misfit dislocations are preferably nucleated in regions with high CdSe contents where the strain exceeds the strain in the surrounding WL. The "coffee-bean" is typically interpreted in terms of coherently strained particles in a matrix [7]. However, the "coffee-bean" contrast, which is observed in our samples under strong-beam conditions (e.g. Fig. 1a), is induced by SFs in combination with the small cap layer thickness of 20 nm. Therefore, the true origin of the contrast can be only resolved in WB images.

The Cd distribution and the arrangement of the SIs in the three-stack structures strongly depends on t_{ZnSe}. For thin spacers (<10 ML) an intermixing of the ZnSe and CdSe layers is observed which is indicative of strong Cd segregation and/or interdiffusion. For the sample with t_{ZnSe}= 12 ML a vertical ordering of the SIs occurs which was similarly observed e.g. in InAs/GaAs structures [8]. The vertically correlated arrangement can be explained by the increased elastic strain around the SIs of the first layer where the local lattice parameter is larger than in the WL. The ZnSe, which is deposited on top of the CdSe, is differently strained according to the underlying CdZnSe, i.e. with a larger lateral lattice parameter on top of the Cd-rich inclusions. The deposition of the second and third CdSe layer can be expected to preferentially occur with a higher x_{Cd} in regions where the ZnSe provides a larger lattice parameter. Therefore, the growth of the correlated SIs is energetically profitable. With increasing t_{ZnSe} the influence of elastic strain at the surface of ZnSe spacer decreases and consequently also the tendency towards a correlated arrangement of the SIs.

5. Summary CdSe/ZnSe QD structures were studied by TEM and RHEED. Strongly broadened wetting layers with a thickness of ≈3 nm independent of t_n and small islands are observed in all samples whose Cd concentration increases with t_n. Large islands, associated with a 2D/3D growth-mode transition at $t_n \approx 2.5$ ML, with a high x_{Cd} are also formed. Stacking faults are generated close to LIs which exhibit a "coffee-bean" contrast in strong-beam plan-view TEM images at small cap layer thicknesses. An intermixing of CdSe and ZnSe is observed in the three-stack structure at $t_{ZnSe} = 10$ ML. A predominant vertical correlation of the SIs occurs for $t_{ZnSe} = 12$ ML. The degree of vertical ordering decreases at larger t_{ZnSe} due to the decreasing influence of the strain exerted by the SIs at the top of the ZnSe buffer layers.

References

[1] H. KIRMSE, R. SCHNEIDER, M. RABE, W. NEUMANN, and F. HENNEBERGER, Appl. Phys. Lett. **72**, 1329 (1998).

[2] D. SCHIKORA, S. SCHWEDHELM, D.J. AS, K. LISCHKA, D. LITVINOV, A. ROSENAUER, D. GERTHSEN, M. STRASSBURG, A. HOFFMANN, and D. BIMBERG, Appl. Phys. Lett. **76**, 418 (2000).

[3] N. Peranio, A. Rosenauer, D. Gerthsen, S.V. Sorokin, I.V. Sedova, and S.V. Ivanov, Phys. Rev. B **61**, 16015 (2000).
[4] T. Kümmell, R. Weingand, G. Bacher, A. Forchel, K. Leonardi, D. Hommel, and H. Selke, Appl. Phys. Lett. **73**, 3105 (1998).
[5] I.L. Krestnikov, M. Strassburg, M. Cesar, A. Hoffmann, U.W. Pohl, D. Bimberg, N.N. Ledentsov, P.S. Kopev, Zh.I. Alferov, D. Litvinov, A. Rosenauer, and D. Gerthsen, Phys. Rev. B **60**, 8695 (1999).
[6] A. Rosenauer and D. Gerthsen, Ultramicroscopy **76**, 49 (1999).
[7] M.F Ashby and L.M. Brown, Phil. Mag. **8**, 1083 (1963).
[8] Q. Xie, A. Madhukar, P. Chen, and N.P. Kobayashi, Phys. Rev. Lett. **75**, 2542 (1995).